PHYSICAL REVIEW LETTERS

Spectral Tuning by Selective Enhancement of Electric and Magnetic Dipole Emission

Sinan Karaveli and Rashid Zia*

School of Engineering, Brown University, Providence, Rhode Island 02912, USA
(Received 5 January 2011; revised manuscript received 8 March 2011; published 11 May 2011)

We demonstrate that magnetic dipole transitions provide an additional degree of freedom for engineering emission spectra. Without the need for a high-quality optical cavity, we show how a simple gold mirror can strongly tune the emission of trivalent europium. We exploit the differing field symmetries of electric and magnetic dipoles to selectively direct the majority of emission through each of three major transitions (centered at 590, 620, and 700 nm), and present a model that accurately predicts this tuning from the local electric and magnetic density of optical states.

It is often assumed that light-matter interactions are mediated by electric fields and that the Lorentz force from optical-frequency magnetic fields may be neglected [1]. A comparison of dipole moments in the Bohr model suggests that magnetic dipole (MD) transitions should be roughly 10^5 times weaker than electric dipole (ED) transitions, and thus, that the relative permeability of natural materials at optical frequencies should be close to 1 [1,2]. Nevertheless, the tremendous success of metamaterials research has helped to upend conventional assumptions about light-matter interactions. The magnetic resonances supported by metal nanostructures, such as split-ring resonators, have allowed researchers to engineer optical metamaterials with negative permeabilities [2]. Researchers have also leveraged the magnetic response from metallized near-field probes to map magnetic fields [3] and study magnetic effects at optical frequencies [4,5].

Despite recent interest in magnetic light-matter interactions, few studies have investigated ways to enhance the role of MD [6,7] and higher-order transitions [8] on the fundamental process of spontaneous emission. Over the past decade, there has been considerable research aimed at controlling the spontaneous emission of ED transitions using resonant cavities [9] and optical antennas [10]. Detailed studies have shown that ED emission can be enhanced by increasing emission rates [11,12] and promoting directional emission [13,14]. Recent studies have also shown that metal cavities [15] and nanoparticle dimers [16] can be used to tune the emission spectra of ED emitters by modifying the wavelength-dependent local density of optical states (LDOS).

Given the perceived dominance of ED transitions, the LDOS is commonly defined in terms of the electromagnetic modes into which an ED may emit [17]. However, strong optical-frequency MD transitions do exist. Lanthanide ions, such as trivalent erbium (Er^{3+}) and europium (Eu^{3+}), exhibit ED and MD transitions of comparable strength [18]. For example, Drexhage, Kunz, and Lukosz used Eu^{3+} to study differences in the modified radiation patterns and rates for ED and MD transitions [19,20]. Eu^{3+} has also been used to study local field effects on ED and MD transitions in dielectrics [21].

In this Letter, we demonstrate that modifications to the electric and magnetic dipole LDOS can be used to tune emission spectra, and thus show how MD transitions provide an additional degree of freedom with which to engineer spontaneous emission. Specifically, we show how differing self-interference effects for ED and MD transitions can be used to tune the emission spectra of Eu^{3+} ions near a planar gold mirror. This work builds on our recent demonstration of enhanced MD emission by inhibiting the dominant ED transition in organic Eu^{3+} chelates [7]. The inorganic Eu^{3+} doped Y_2O_3 thin films used in this study exhibit several strong transitions from 580 to 715 nm, and thereby enable investigation of emission tuning over a large spectral range. Without the need for a strong optical resonance, we show that controlling the emitter-metal separation distance allows us to selectively direct over 50% of observed emission through each of the three major transitions, i.e., the MD transition at 590 nm and two ED transitions at 620 and 700 nm. Furthermore, we demonstrate that this broad spectral tuning is predicted by a multilevel emitter model that couples the appropriate electric and magnetic dipole LDOS factors.

Schematics of the studied samples are shown in the insets of Fig. 1. Samples were fabricated by depositing a 20 nm Eu^{3+}:Y_2O_3 emitter layer onto a set of quartz coverslips using rf-magnetron cosputtering of Eu_2O_3 and Y_2O_3. The samples were then annealed in O_2 at 1000 °C for 1 h. Different thickness Al_2O_3 spacer layers were deposited by reactive sputtering of Al with a 1:9 (O_2:Ar) gas mixture, and layer thicknesses confirmed by ellipsometry. Finally, a 3 nm Ti adhesion layer and 100 nm Au film were deposited with electron-beam evaporation onto half of each sample to produce metal coated and uncoated regions for each spacer layer thickness. Photoluminescence under 532 nm laser excitation was studied with a grating spectrograph. Samples were excited and emission collected from the quartz side using a 0.85 numerical aperture (NA) objective.
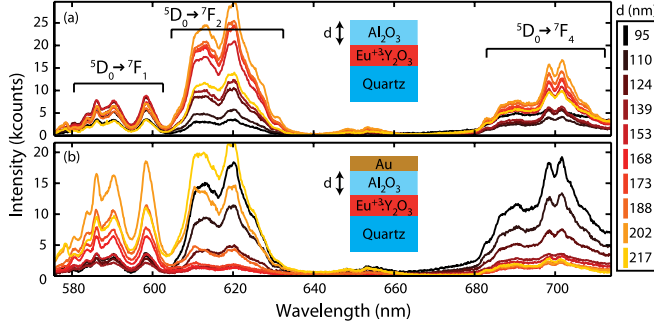
FIG. 1 (color online). Emission spectra measured from (a) uncoated and (b) gold-coated regions of $Eu^{3+}:Y_2O_3$ thin film samples with Al_2O_3 spacer layers of varying thickness d. Spectra demonstrate strong modification over a broad wavelength range. Insets: Schematic of fabricated structure.

Figure 1 shows emission spectra of $Eu^{3+}:Y_2O_3$ for different Al_2O_3 spacer layers thicknesses with and without the gold mirror. The three major transitions are the $^5D_0 \rightarrow {^7F_1}$ MD transition from 580–603 nm, $^5D_0 \rightarrow {^7F_2}$ ED transition from 603–635 nm, and $^5D_0 \rightarrow {^7F_4}$ ED transition from 680–715 nm. These transitions are labeled according to the dominant Russell-Saunders ($^{2S+1}L_J$) terms in the intermediate coupling configuration of $4f^6$ valence electrons in Eu^{3+} [22]. In intermediate coupling, the $^5D_0 \rightarrow {^7F_1}$ ($\Delta J = 1$) is allowed by the MD selection rule, whereas the $^5D_0 \rightarrow {^7F_{2,4}}$ ($\Delta J = 2, 4$) ED transitions are mediated by crystal-field effects. The multiple peaks observed for each transition are associated with splitting of the ^7F_J ground states (e.g., $^7F_1$ may split into 3 states with $M_J = 0, \pm 1$). Importantly, these three major transitions are connected to each other via the shared $^5D_0$ excited state from which they originate. Although the emitter layer of each sample is identical, Fig. 1 shows that the emission spectra vary significantly, especially for the gold-coated regions. Comparing Figs. 1(a) and 1(b), differences can be observed in how the uncoated and coated spectra change with the spacer layer thickness, d. For example, as d increases from 95 to 200 nm, the intensity of the $^7F_4$ transition increases for the uncoated regions, but decreases for the gold-coated regions.

The large spectral modification due to the gold mirror can be quantified by analyzing the branching ratios for the three major transitions as a function of d. The experimental branching ratio $\beta_J(d)$ is defined as the fraction of total observed intensity mediated by each transition: $\beta_J(d) = \int_{\lambda_J} I(\lambda, d) d\lambda / \int I(\lambda, d) d\lambda$, where $I(\lambda, d)$ is the measured intensity at each wavelength for a given spacer layer thickness. The integral in the numerator is taken over the wavelength range of each ^7F_J transition, while the denominator is integrated over the full spectral range. This normalization eliminates pump interference effects which modulate the total fluorescence intensity. Figure 2(a) shows that different spacer layer thicknesses can be used to selectively direct over 50% of observed light emission through each transition. The dominant emission peak
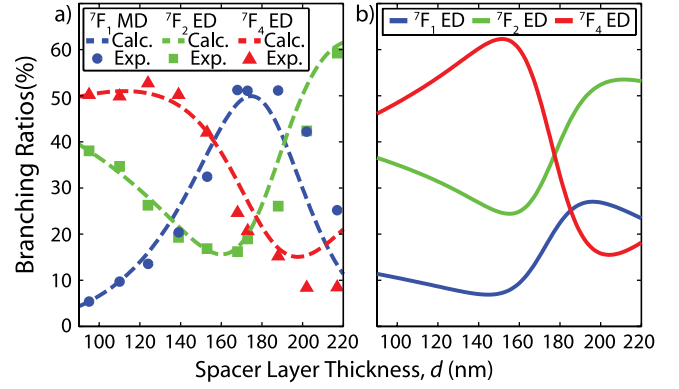

FIG. 2 (color online). (a) Experimental (dots, squares, and triangles) and theoretical (dashed lines) branching ratios for the $^7F_1$ (blue), $^7F_2$ (green), and $^7F_4$ (red) transitions as a function of spacer thickness for gold-coated samples. (b) Theoretical calculations for the hypothetical case where the $^7F_1$ transition is mediated by an ED, rather than MD, transition.

changes from the $^7F_4$ ED transition ($d < 140$ nm) to the $^7F_1$ MD transition ($d \sim 170$ nm) to the $^7F_2$ ED transition ($d > 210$ nm). The experimental branching ratios for the two ED transitions ($^7F_2$ and $^7F_4$) both exhibit relative minima in Fig. 2(a), but the minima are shifted by ~ 40 nm due to their different emission wavelengths. The $^7F_1$ MD transition, however, follows the opposite trend and shows a relative maxima between the minima of the two ED transitions. This difference between ED and MD transitions is critical to the broad spectral tuning that we observe and is due to the π-phase difference between reflected electric and magnetic fields as discussed below.

To understand and predict the observed spectral modification, we use classical self-interference theory to model the radiation emitted by these dipolar transitions [23]. Each Eu^{3+} transition is modeled as an isotropic ED or MD emitter located within a planar three-layer structure. Changes to the radiative decay rates Γ^{ED} and Γ^{MD} are derived in terms of the reflected electric and magnetic fields, respectively. When the reflected field is in phase with the emitted field at the dipole location, radiative decay is enhanced; when out of phase, radiative decay is inhibited. Using the formulation in Ref. [23], the normalized radiative decay rates are calculated as follows:

$$\frac{\Gamma^{ED}}{\Gamma_0} = \frac{1}{2} \text{Im} \left[\int_0^{u_{max}} \left(\frac{(1 + R_{12}^s)(1 + R_{13}^s)}{1 - R_{12}^s R_{13}^s} \right. \right.$$
$$\left. \left. + \frac{(1 + R_{12}^p)(1 + R_{13}^p) - 2u^2(R_{12}^p + R_{13}^p)}{1 - R_{12}^p R_{13}^p} \right) \frac{u \, du}{l_1} \right],$$
$$(1)$$

$$\frac{\Gamma^{MD}}{\Gamma_0} = \frac{1}{2} \text{Im} \left[\int_0^{u_{max}} \left(\frac{(1 - R_{12}^p)(1 - R_{13}^p)}{1 - R_{12}^p R_{13}^p} \right. \right.$$
$$\left. \left. + \frac{(1 - R_{12}^s)(1 - R_{13}^s) + 2u^2(R_{12}^s + R_{13}^s)}{1 - R_{12}^s R_{13}^s} \right) \frac{u \, du}{l_1} \right],$$
$$(2)$$

where $R_{ij}^{s,p} = r_{ij}^{s,p} \exp(-2kl_i s_{ij})$ represents the reflected electric field from the i, j interface at the emitter's location. $r_{i,j}^s = (l_i - l_j)/(l_i + l_j)$ and $r_{i,j}^p = (\varepsilon_i l_j - \varepsilon_j l_i)/(\varepsilon_i l_j + \varepsilon_j l_i)$ are the reflection coefficients for s and p polarization, and s_{ij} is the distance of the emitter from the i, j interface. The subscript index 1 designates the central layer in which the emitter is embedded, while indices 2 and 3 represent the bottom and top layers, respectively. In modeling our experiments, the central region consisting of $Eu^{3+}:Y_2O_3$ and Al_2O_3 is approximated by the refractive index of Al_2O_3 ($n_1 = 1.68$). The emitter distance from the quartz substrate ($n_2 = 1.46$) is fixed at $s_{12} = 20$ nm, and the emitter distance from the gold (with index n_3 modeled by the Brendel-Bormann model [24]) is varied with the Al_2O_3 spacer thickness such that $s_{13} = d$. Γ_0 is the emission rate in a homogeneous medium with index n_1. $u = k_\parallel/k$ and $l_j = -i\sqrt{n_j^2/n_1^2 - u^2}$ are the parallel and perpendicular components of the wave vector normalized to the emitter layer wave number, $k = (2\pi/\lambda)n_1$. The upper bound of integration u_{max} can be used to account for the finite collection efficiency of the optical system. By setting $u_{max} = NA/n_1$, Eqs. (1) and (2) approximate the normalized emission rate into the optical modes collected by a finite NA [25]. Alternatively, by setting $u_{max} = \infty$, Eqs. (1) and (2) are proportional to the total number of optical modes into which an ED and MD may emit. When multiplied by the homogeneous density of optical states, they represent three-layer equivalents to the electric and magnetic LDOS as defined in Ref. [26] for a two-layer planar structure.

Qualitatively, the definition of $R_{ij}^{s,p}$ shows how self-interference effects depend on three important parameters: emission wavelength, emitter location, and dipole nature. Together, the emission wavelength and emitter location determine the phase acquired by the reflected field during propagation to and from the interfaces. This explains the minima shift observed with respect to d for the two ED transitions in Fig. 2(a): destructive self-interference of the $^7F_2$ transition occurs for a thinner spacer layer thickness than the longer wavelength $^7F_4$ transition. The dipole nature determines whether electric or magnetic fields define the self-interference effects. Note that Eq. (2) may be obtained by interchanging $R_{i,j}^s$ with $-R_{i,j}^p$ in Eq. (1) to account for the π-phase and polarization differences between reflected electric and magnetic fields. Hence, MD emission tends to be enhanced at wavelengths and distances for which ED emission is suppressed, as evidenced by the opposite symmetry of MD and ED branching ratios in Fig. 2(a).

Quantitatively, Eqs. (1) and (2) can be used to directly predict the experimental branching ratios and emission spectra. The normalized emission spectra $NI(\lambda, d) = I(\lambda, d)/\int I(\lambda, d)d\lambda$ can be defined in terms of the radiative decay rates as $NI(\lambda, d) = \Gamma(\lambda, d)/\int \Gamma(\lambda, d)d\lambda$, where $\Gamma(\lambda, d)$ is the appropriate ED or MD radiative decay rate

at each wavelength and spacer layer thickness. This definition accounts for coupling between transitions in this multilevel system; i.e., the fractional intensity at each wavelength depends on the rate of all radiative transitions originating from the $^5D_0$ excited state [7]. If the homogeneous decay rate at each wavelength $\Gamma_0(\lambda)$ was known, $NI(\lambda, d)$ could be calculated directly using Eqs. (1) and (2). Alternatively, one can use the measured spectra from any known inhomogeneous sample as a reference case. Defining the ratio of radiative decay rates as a relative LDOS enhancement factor, $F(\lambda, d, d_{ref}) = \Gamma(\lambda, d)/\Gamma(\lambda, d_{ref})$, we can reformulate an expression for the normalized spectra in terms of the experimental emission spectra of a known reference as

$$NI(\lambda, d) = \frac{F(\lambda, d, d_{ref})NI(\lambda, d_{ref})}{\int F(\lambda, d, d_{ref})NI(\lambda, d_{ref})d\lambda}. \qquad (3)$$

Equation (3) may be used to directly predict the normalized emission spectrum $NI(\lambda, d)$ at any spacer layer distance d, or it may be used to infer the normalized emission spectrum in a homogeneous environment by selecting the special case where $F(\lambda, d_{ref}) = \Gamma_0(\lambda)/\Gamma(\lambda, d_{ref})$.

Figure 3 shows the gold-coated $NI(\lambda, d)$ as predicted by Eq. (3) alongside the experimental spectra measured for three representative spacer layer thicknesses [27]. For these calculations, the spectrum from the gold-coated region of the 95 nm spacer layer sample was used as a reference ($d_{ref} = 95$ nm), and enhancement factors $F(\lambda, d, d_{ref})$ calculated with $u_{max} = 0.85/1.68$ in Eqs. (1) and (2) to approximate the collection efficiency of our 0.85 NA objective. There is strong agreement between theory and experiment for the 110 and 173 nm samples. Despite deviations for the thicker 217 nm sample, the theoretical spectrum accurately predicts the dominant $^7F_2$ transition. To highlight spectral changes, Fig. 3 also shows the inferred homogeneous spectrum.
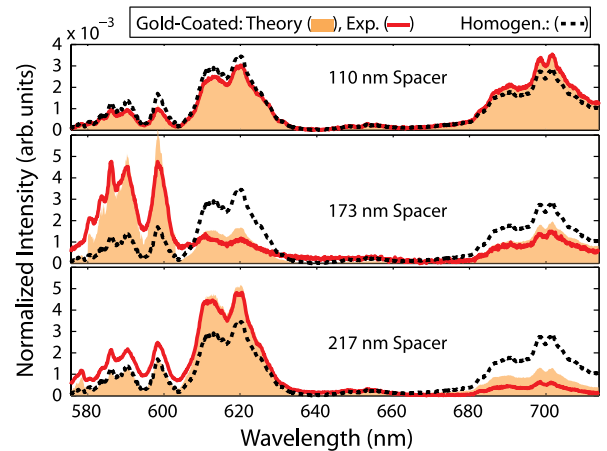

FIG. 3 (color online). Normalized emission spectra of gold-coated samples. Comparison of experimental data (solid line) with theoretical predictions based on Eq. (3) (shaded region) and inferred homogeneous spectrum (dashed line).

Equation (3) may also be integrated over the spectral range of each transition to predict the branching ratio: $\beta_J(d) = \int_{\lambda_J} NI(\lambda, d)d\lambda$. The dashed lines in Fig. 2(a) show theoretical $\beta_J(d)$ values calculated using the aforementioned reference spectrum. Comparison with experimental data shows good agreement for all three transitions. In particular, the theory captures how the relatively weak $^7F_1$ MD transition becomes the dominant transition for d between 160 and 190 nm. As a point of comparison, the branching ratios for the inferred homogeneous spectrum are 14%, 39%, and 41% for the $^7F_1$, $^7F_2$, and $^7F_4$ transitions, respectively. This means that we observe a greater than threefold enhancement in MD branching ratio. Although this measured enhancement depends on collection efficiency, our theoretical model continues to predict strong spectral tuning for larger NA values. For example, if we were to collect all the far-field radiation emitted into air (NA = 1), the predicted branching ratio for the $^7F_1$ MD transition would still exceed 40% [28].

To prove that this spectral tuning strongly relies on the MD nature of the $^7F_1$ transition, Fig. 2(b) shows the branching ratios predicted if all three transitions were mediated by EDs. The curves were obtained using the same reference and method as Fig. 2(a), but assuming the $^7F_1$ transition to be an ED when calculating the normalized spectra with Eq. (3). For this hypothetical case, the stronger $^7F_2$ and $^7F_4$ transitions always remain dominant, and the $^7F_1$ branching ratio never exceeds 30%. Because of the spectral proximity of the $^7F_1$ transition centered at 590 nm and $^7F_2$ transition centered at 620 nm, any enhancement to the former is always overshadowed by similar enhancement to the latter. In contrast to the resonant cavity in Ref. [15], the simple structure considered here does not have a sufficiently high quality factor to selectively enhance just one of two close ED transitions [29]. Nonetheless, our experiments show that a high quality factor is not required to distinguish these two close transitions in Eu^{3+} because the differing self-interference effects for ED and MD transitions provide an additional mechanism by which to engineer emission.

In summary, we have demonstrated broad spectral tuning using a simple metal mirror to modify the optical modes available to the ED and MD transitions of Eu^{3+}. By varying the distance of the emitter layer from the mirror, we can direct over 50% of observed light emission through any of three transitions spanning over a 100 nm spectral range. Experimental results show good agreement with a multilevel model that couples the LDOS enhancement factors of competing transitions, and we demonstrated that the observed spectral changes depend strongly on differences between ED and MD emission.

These results highlight a simple means by which to engineer the emission of lanthanide ions, which serve as important emitters in a range of technologies from lighting and displays to lasers and fiber amplifiers. Moreover, by showing that a majority of observed emission in a stable inorganic material can be mediated by MD transitions, these experiments open the possibility for new active measurements of magnetic light-matter interactions. Experiments using such naturally occurring MD emitters could complement recent studies based on the artificial magnetic resonances of metal nanostructures [2–5].

---

*Rashid_Zia@brown.edu

[1] H. Giessen and R. Vogelgesang, Science **326**, 529 (2009).
[2] V. M. Shalaev, Nat. Photon. **1**, 41 (2007).
[3] M. Burresi et al., Science **326**, 550 (2009).
[4] M. Burresi et al., Phys. Rev. Lett. **105**, 123901 (2010).
[5] S. Vignolini et al., Phys. Rev. Lett. **105**, 123902 (2010).
[6] N. Noginova et al., Opt. Express **17**, 10 767 (2009).
[7] S. Karaveli and R. Zia, Opt. Lett. **35**, 3318 (2010).
[8] M. L. Andersen et al., Nature Phys. **7**, 215 (2010).
[9] K. J. Vahala, Nature (London) **424**, 839 (2003).
[10] P. Bharadwaj, B. Deutsch, and L. Novotny, Adv. Opt. Photon. **1**, 438 (2009)
[11] S. Kühn et al., Phys. Rev. Lett. **97**, 017402 (2006).
[12] P. Anger, P. Bharadwaj, and L. Novotny, Phys. Rev. Lett. **96**, 113002 (2006).
[13] T. H. Taminiau et al., Nat. Photon. **2**, 234 (2008).
[14] A. G. Curto et al., Science **329**, 930 (2010).
[15] A. Chizhik et al., Phys. Rev. Lett. **102**, 073002 (2009).
[16] M. Ringler et al., Phys. Rev. Lett. **100**, 203002 (2008).
[17] Even for emitters such as erbium that support both ED and MD transitions, e.g., E. Snoeks, A. Lagendijk, and A. Polman, Phys. Rev. Lett. **74**, 2459 (1995).
[18] W. T. Carnall, P. R. Fields, and K. Rajnak, J. Chem. Phys. **49**, 4412 (1968).
[19] K. H. Drexhage, Prog. Opt. **12**, 163 (1974).
[20] R. E. Kunz and W. Lukosz, Phys. Rev. B **21**, 4814 (1980).
[21] G. L. J. A. Rikken and Y. A. R. R. Kessener, Phys. Rev. Lett. **74**, 880 (1995).
[22] G. S. Ofelt, J. Chem. Phys. **37**, 511 (1962); **38**, 2171 (1963).
[23] R. Chance, A. Prock, and R. Silbey, Adv. Chem. Phys. **37**, 1 (1978).
[24] A. D. Rakic et al., Appl. Opt. **37**, 5271 (1998).
[25] This formulation is exact for collection from both half-spaces. As light is reflected in the presence of the gold mirror, it may also approximate collection from one side.
[26] K. Joulain et al., Phys. Rev. B **68**, 245405 (2003).
[27] See supplemental material at http://link.aps.org/supplemental/10.1103/PhysRevLett.106.193004 for complete set of spectra.
[28] Calculation of the total emitted power ($u_{max} = \infty$) yields a 20% branching ratio for the MD transition. However, this value includes radiation into waveguide and surface modes that are not readily observed in the far field.
[29] The cavity formed by reflections from the Au film and the Al_2O_3/SiO_2 interface has a quality factor between 1 and 3 depending on the wavelength and spacer thickness.